International Journal of Minerals, Metallurgy and Materials
Volume 26, Number 2, February 2019, Page 234
https://doi.org/10.1007/s12613-019-1728-6

Facile synthesis of flake-like dihydrate zinc oxalate particles

Xing Chen[1,2], *Xin Liu*[1], *and Kai Huang*[1,3]

1) School of Metallurgical and Ecological Engineering, University of Science and Technology Beijing, Beijing 100083, China

2) Global Energy Research Institute, Future Science and Technology Park, Beijing 102211, China

3) Beijing Key Lab of Green Recycling and Extraction of Metals, University of Science and Technology Beijing, Beijing 100083, China

(Received: 7 April 2018; revised: 23 May 2018; accepted: 27 May 2018)

Abstract: Monodispersed dihydrated zinc oxalate ($ZnC_2O_4·2H_2O$) particles with characteristic morphology were synthesized by aging a mixed solution of zinc nitrate ($Zn(NO_3)_2$) and sodium oxalate ($Na_2C_2O_4$) in the presence of a citrate ligand, with an average flat size of approximately 10–15 μm. The important parameters, including the solution pH values and the concentration of the zinc ions and citrate ligand, were investigated using a series of experiments. It is verified that the citrate ligand significantly affects the morphology of zinc oxalate particles, probably via its multiple roles of chelating, dispersing, and selective absorption. Thermodynamic equilibrium of the distribution of zinc species in an aqueous solution of Zn(II)–citrate–oxalate–H_2O was estimated to explain the experimental results and to clarify the size and morphological evolution mechanism of the precipitated particles.

Keywords: facile synthesis; zinc oxalate; flaky morphology; citrate ligand; one-pot synthesis

1. Introduction

The controlled synthesis of various inorganic fine particles with specific size, shape, and structure is considerably significant in the modern material science and industry fields such as catalysis, medicine, electronics, ceramics, pigments, cosmetics, and so on [1–6]. As compared with the controlling of particle size, morphological controlling appears to be more difficult because the number of relevant theories related to morphological controlling is much more scarce as compared to those of size controlling [7–10]. Some common empirical laws, such as the LaMer law [11], Weimarn law [12–13], and Ostwald ripening law [14–16], majorly focus on size controlling; only Ostwald law mentions a few aspects related to the sphericationor surface smoothing of the precipitated particles by performing the dissolution–recrystallization process, which is related to the shape or morphology of particles [17]. Considering the fact that the morphology of particles usually influences final products' properties, various methods, such as designing special solution systems, setting the specific precipitation conditions, using template-induced techniques with polymers or seeding, and so on, have been developed to tailor the morphology of precipitated particles [18–20]. Actually, almost all of the aforementioned measures should be considered during the practical synthesis processes.

As for the zinc oxalate precipitation system, it has been quite popularly adopted to prepare the precursor of zinc oxide particles, which are well-recognized to form excellent semiconductor materials when applied to the fields of photocatalysis, ultraviolet-screening, electric ceramics, and so on [21–23]. Several researchers have paid attention to the preparation of zinc oxalate particles with various shapes [21–22,24–26]. Few reports have studied zinc oxalate with a flaky morphology, which may be a good precursor for the preparation of flaky zinc oxide particles that can be used as ultraviolet-light shelding materials. In this study, we developed a simple solution system of aging in a one-pot manner and synthesized monodispered zinc oxalate particles with a flaky morphology in the presence of a citrate ligand, which may act as (1) a chelating reagent to control the precipitation process, (2) a dispersing reagent to prevent the precipitated particles from serious aggregation, and (3) a crystal mor-

Corresponding author: Kai Huang E-mail: khuang@metall.ustb.edu.cn

phology modifier by selective absorption on the special crystalline facets.

2. Experimental

2.1. Preparation

All the reagents were of analytical grade and were used without any further purification. Deionized water was used during the synthesis and treatment processes. Citric acid, zinc nitrate ($Zn(NO_3)_2$), and sodium oxalate ($Na_2C_2O_4$) were obtained from the Sinopharm Chemical Reagent Co., Ltd., Beijing, China.

In a standard synthesis procedure, an aqueous solution of $Na_2C_2O_4$ (0.1 mol/L, 30 mL), $Zn(NO_3)_2$ (0.1 mol/L, 30 mL), and citric acid (10 g/L, 10 mL) was quickly injected into 930 mL of deionized water. The solution was then stirred magnetically for 2 min to attain a homogeneous state, and the pH value was adjusted to 6.5 using either dilute sodium hydroxide (NaOH) or nitric acid (HNO_3) solution. This resulted in a final ZnC_2O_4 concentration of 3 mmol/L in the solution. This mixture was sealed in a beaker and kept undisturbed for 12 h in an oven, after which the precipitate was collected by centrifugation. In a systematical study, the final concentration of ZnC_2O_4 varied from 2 to 5 mmol/L, while the solution pH values varied from 3.5 to 7.5.

2.2. Characterization

The prepared precipitates were washed with deionized water and anhydrous alcohol and were further dried at 60°C overnight. The particle samples were characterized by scanning electron microscopy (SEM) (Zeiss Supra55, Germany) with an accelerating voltage of 20 kV. The powder X-ray diffraction (XRD) patterns that were obtained by an X-ray diffractometer (Rigaku FEN-100, Japan) using the Cu K_α radiation at a scan rate of 10°/min, were used to identify any phases and the crystallite size. The accelerating voltage and applied current were 35 kV and 20 mA, respectively. The differential scanning calorimetry–thermogravimetry (DSC–TG) was performed using a TG–DSC instrument (Netzsch STA-449, Germany) under an air flow of 100 mL/min with a heating rate of 10°C/min from room temperature to 500°C.

3. Results and discussion

3.1. Effect of citrate

It can be observed from Fig. 1(a) that, even in the absence of a citrate ligand, the obtained precipitates exhibit a flaky shape although they are not uniform in terms of size

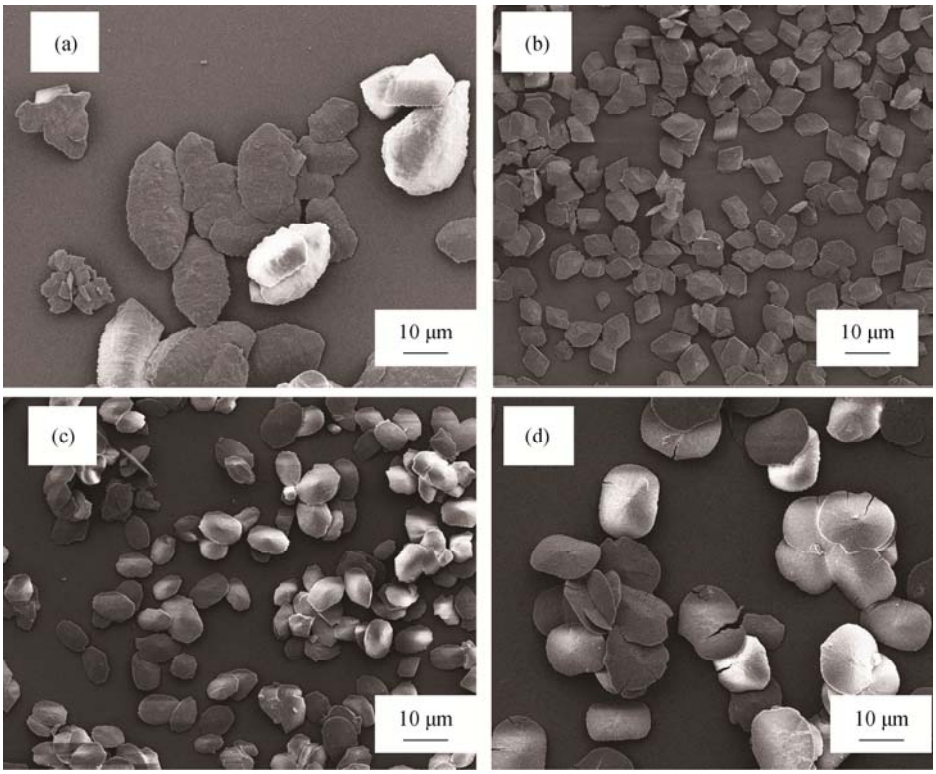

Fig. 1. SEM images of the zinc oxalate particles obtained at an initial ZnC_2O_4 concentration of 3 mmol/L and pH 6.5 in the presence of different sodium citrate concentrations for different aging times: (a) 0 g/L for 24 h; (b) 0.1 g/L for 24 h; (c) 0.2 g/L for 24 h; (d) 0.4 g/L for 48 h.

and morphology. The appearance of a flaky shape can be ascribed to the very dilute concentration of the zinc ions and oxalate anions at the level of several mmol/L. The addition of citrate ligand made the flaky zinc oxalate particles monodispersed and small in size, as demonstrated in Figs. 1(b) and 1(c). This can be explained by the fact that, in the presence of an appropriate amount of citrate, the zinc ions will be slowly released for precipitation due to the chelating affinity between the zinc species and citrate. The results also exhibited that the different induction period times, which can be defined as the moment of appearance of the turbid precipitates, will be drastically prolonged at a higher concentration of citrate. According to the famous LaMer law [12–13], slow precipitation is effective for the separation of the nucleation and growth stages, which further promotes the formation of monodipersed particles. Based on these observations, we deduced that citrate ligands were probably adsorbed onto a certain crystalline facet of the zinc oxalate particles. This process limited the particles' perpendicular growth and caused the formation of a flaky morphology, as depicted in Fig. 1(d), in which the citrate concentration was set to be as high as 0.4 g/L. Under these conditions, no precipitation occured in the initial 24 h; thus, 48 h was required to induce precipitation.

To clarify the formation mechanism of the precipitate that has been described above, the percentages of various zinc species in the aqueous solution of Zn(II)–citrate–oxalate–H_2O were calculated based on the thermodynamic equilibrium principles [27] and were sketched by referring to similar experimental conditions. Fig. 2 illustrates that, in a pH range of approximately 1–14, the presence of citrate will lead to the formation of Zn(II)–citrate complex with a higher concentration of citrate, which will influence the precipitation of zinc ions with oxalate. As depicted in the figures, $Zn(cit)^-$ predominates in the pH range of 4 to 9. Thus, under a pH value of 6.5 in the experiments, the $Zn(cit)^-$ may influence the nucleation and growth of precipitates by chelation and selective adsorption onto the crystalline facets of the tiny particles.

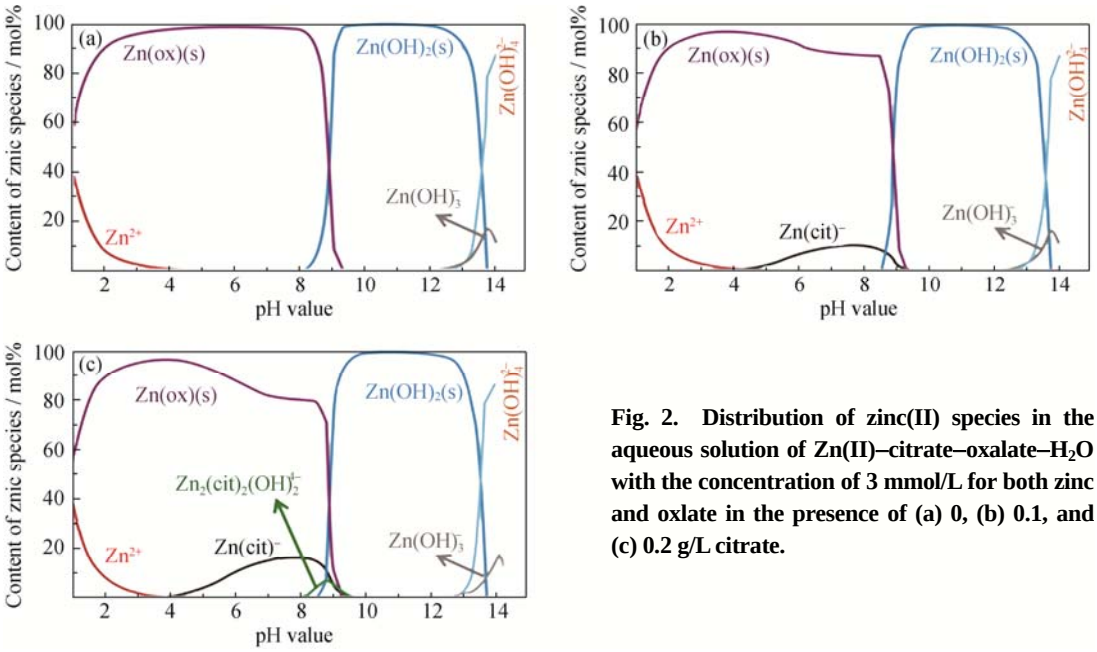

Fig. 2. Distribution of zinc(II) species in the aqueous solution of Zn(II)–citrate–oxalate–H_2O with the concentration of 3 mmol/L for both zinc and oxlate in the presence of (a) 0, (b) 0.1, and (c) 0.2 g/L citrate.

Fig. 3 depicts the X-ray powder diffraction (XRD) patterns of the zinc oxalate particles that are obtained at different concentrations of citrate. It can be observed that all the as-prepared particles were $ZnC_2O_4{\cdot}2H_2O$, corresponding to that observed in the standard crystalline phase well-described by JCPDS No.25-1029. The presence of a citrate ligand drastically promoted the intensity of planes <021>, <020>, <022>, and <130> while inhibiting that of planes <$\bar{2}$02>, <002>, and <$\bar{4}$02>. It can be clearly deduced that the selective adsorption of citrate ligand onto the different crystalline planes of zinc oxalate caused the formation of a flaky shape.

3.2. Fourier-transform infrared spectroscoy (FTIR)

Fig. 4 depicts the FTIR curves of the dihydrate zinc oxalate powders that were prepared both in the absence and presence of 0.1 g/L citrate. It can be observed that both the curves are quite similar except for the drastic intensification at the three peaks located at the wave numbers of 1320, 1364, and 1635 cm^{-1}, which can be attributed to the vibration of the –COO– bonds that is enhanced in the presence of citrate during the precipitation process. It indicates that the

citrate ligand may have become one component of the precipitated particles while its own –COOH ligands enhanced the vibration of the –COO– bonds.

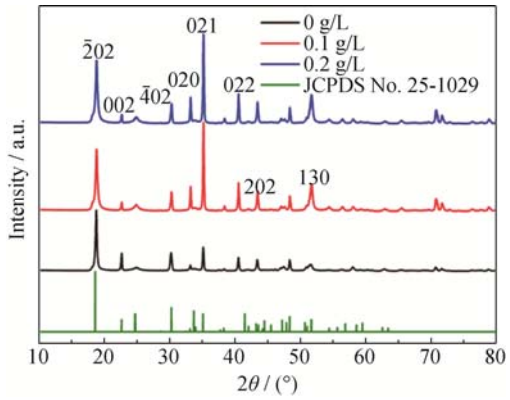

Fig. 3. XRD patterns of the zinc oxalate particles under the following aging conditions: initial ZnC_2O_4 concentration of 3 mmol/L; pH 6.5; aging time of 24 h; and sodium citrate concentrations of 0, 0.1 and 0.2 g/L.

3.3. Effect of pH value

Fig. 5 depicts the effect of the solution pH value on the size and morphology of the dihydrate zinc oxalate particles, and it can be observed that the pH value considerably affects the monodispersity and particle size. At pH 3.5, the obtained particles were typically flaky while they appeared a little aggregated, whereas they become more regular in morphology and better dispersed at pH 4.5. At pH 5.5, the size of the particles became larger; further, subunits with considerably small size are observed in this case, which is clearly the result of secondary nucleation. In case of higher pH values, it can be observed that the preparation of dihydrate zinc oxalate particles at pH 6.5 yielded optimal uniformity in terms of size and morphology. Referring to Fig. 2(b), it is easy to observe that, among the pH values of 3.5, 4.5, 5.5, and 6.5, the effect of $Zn(cit)^-$ can be observed only at a pH value greater than 4.0. The aforementioned four samples seemed to exhibit no significant differences in terms of morphology and size.

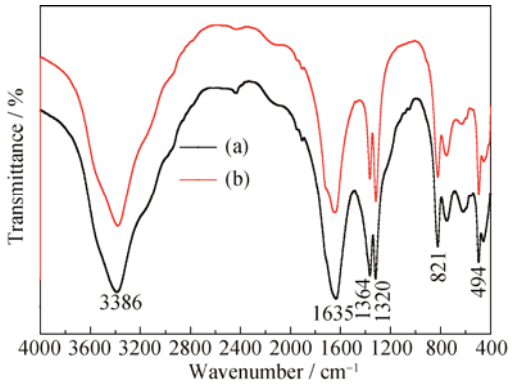

Fig. 4. FTIR curves of the zinc oxalate particles obtained by aging the solution under the following conditions: initial ZnC_2O_4 concentration of 3 mmol/L; pH 6.5; aging time of 24 h; and in the presence of (a) 0 g/L and (b) 0.1 g/L of sodium citrate, as described in Figs. 1(a) and 1(b).

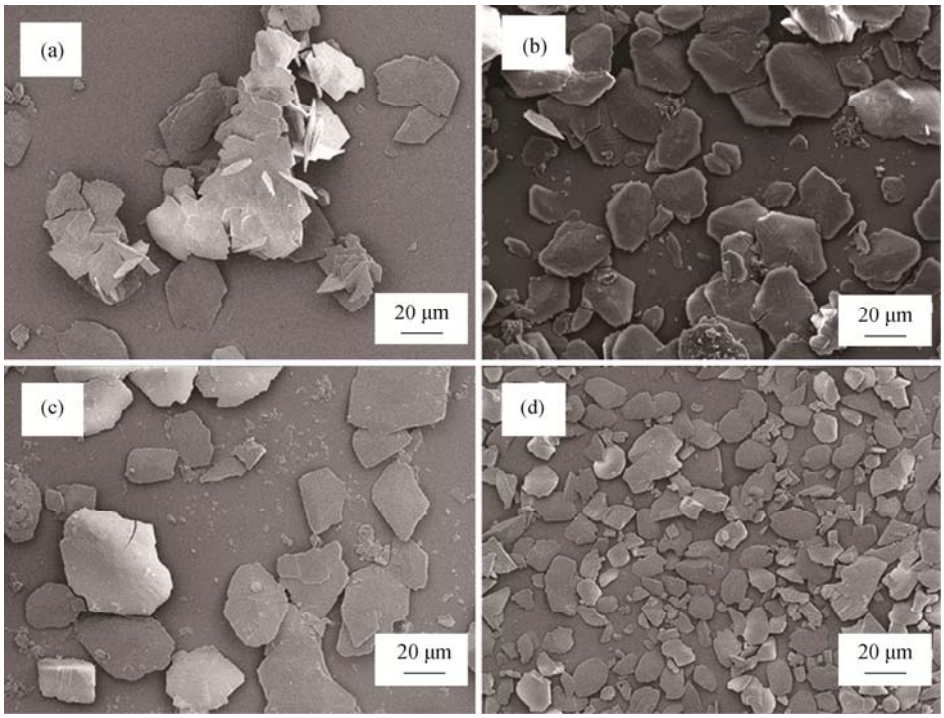

Fig. 5. SEM images of the zinc oxalate particles obtained at an initial ZnC_2O_4 concentration of 3 mmol/L for 24 h in the presence of 0.1 g/L sodium citrate at different pH values: (a) 3.5; (b) 4.5; (c) 5.5; (d) 7.5.

3.4. Effect of zinc(II) concentration

Fig. 6 depicts the SEM photographs of the dihydrate zinc oxalate particles prepared at different initial concentrations of the zinc ion. It can be observed that the precipitated particles were monodispersed micro-sized flakes, whereas they became aggregated into larger particles with irregular morphology, as depicted in Fig. 6(c), with increasing metal ion concentration. It was also observed that, in 2 mmol/L ZnC_2O_4, tiny particles coexisted with the large ones, which can be considered to be the growth units for the formation of larger particles, probably through Ostwald ripening.

3.5. Scaling-up of the preparation

To verify the reproducibility of the precipitation on a large scale, a 10-L volume of the final precipitation solution system was built; the obtained particles are presented in Fig. 7. It can be observed that, mostly, the obtained particles are quite monodispersed with a special flaky morphology and are almost similar to those obtained in the small vessels having a volume of 1 L. Therefore, we deduce that the scaling-up of the present precipitate solution system can be easily achieved. Further, during the exprimental process, it was interesting to observe that the solution process was easier to control and to be kept stable for various parameters, clearly favorable for the reproducible tailoring of particle size and morphology, in a larger-volume precipitation system.

3.6. TG–DSC results of the dihydrate zinc oxalate

The dihydrate zinc oxalate particle samples that were obtained in the absence and presence of citrate were used to test their decomposition behavior in flowing air at a rate of 10 mL/min and 10°C/min, as demonstrated in Fig. 8. It was

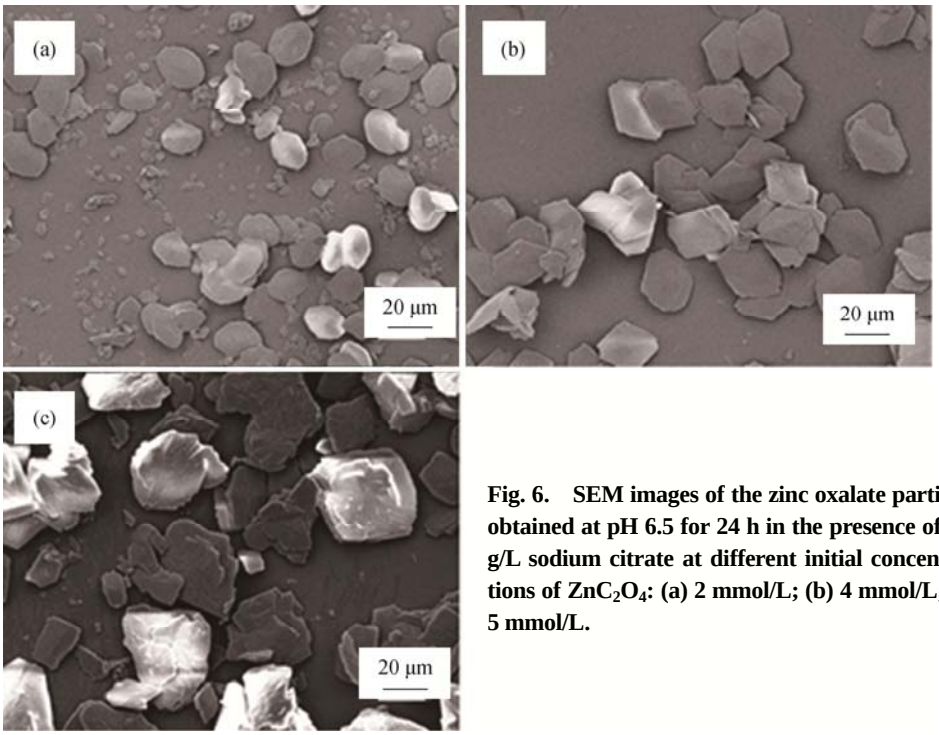

Fig. 6. SEM images of the zinc oxalate particles obtained at pH 6.5 for 24 h in the presence of 0.1 g/L sodium citrate at different initial concentrations of ZnC_2O_4: (a) 2 mmol/L; (b) 4 mmol/L; (c) 5 mmol/L.

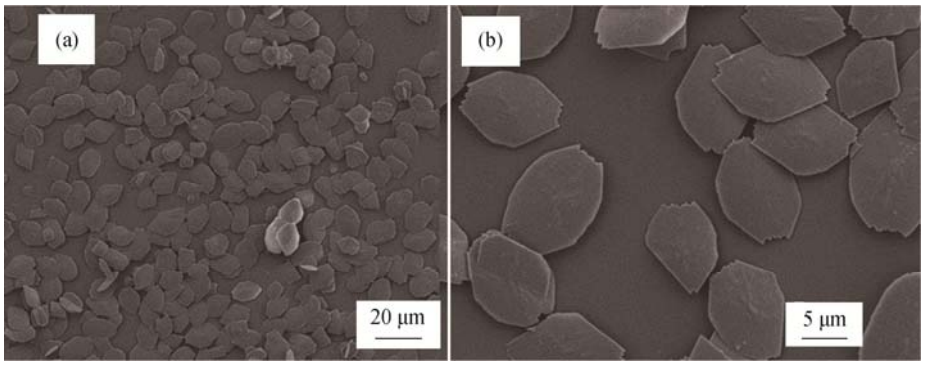

Fig. 7. SEM images of the zinc oxalate particles obtained at an initial ZnC_2O_4 concentration of 3 mmol/L in the presence of 0.1 g/L sodium citrate at pH 6.5 for 24 h in a large-scale volume of 10 L.

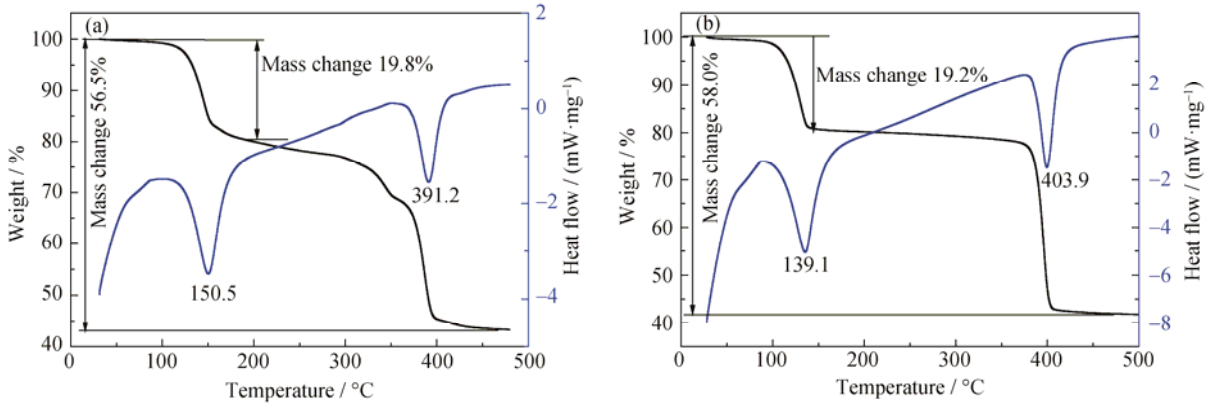

Fig. 8. TG–DSC curves of the zinc oxalate particles obtained by aging the solution under the following conditions: initial ZnC_2O_4 concentration of 3 mmol/L; pH 6.5; aging time of 24 h; and in the presence of sodium citrate of (a) 0 g/L and (b) 0.1 g/L.

observed that both the samples exhibited two obvious mass loss steps, i.e., at temperature peaks of 150 and 139°C, respectively, for the aforementioned samples, which can be deduced as the following decomposition reaction: $ZnC_2O_4{\cdot}2H_2O = ZnC_2O_4 + 2H_2O\uparrow$ (19.0% mass loss in theoretical calculation). It is confirmed that the introduction of citrate precisely helps to decrease the dehydration temperature by at least 10°C, indicating that citrate plays an important role in the formation of crystalline dihydrate zinc oxalate particles and that it may result in loose crystal stacking structure for easier decomposition. The decomposition percentages at temperatures near 400°C for the two samples were 36.7% and 38.8%, respectively, both of which were close to the theoretical decomposition ratio of 38.1% for the decomposition reaction of $ZnC_2O_4 + 0.5O_2 = ZnO + 2CO_2\uparrow$, indicating that the products after thermolysis at 400°C air should be in the pure ZnO phase.

3.7. Formation mechanism of monodispersed particles

For the preparation of monodispersed precipitates, the LaMer law has always been used to design the synthesis system. Based on the model's main assumptions, the concentration of the solution is quite important during the production of uniform particles due to the distinct separation of the nucleation and growth stages by modifying the supersaturation level of the precursor for precipitation. Therefore, very dilute solutions were most often adopted in this study at several mmol/L as shown in Fig. 6 to prevent uncontrollable nucleation phenomena during the growth stage of primary nuclei. The addition of a citrate ligand is effective to perform the aforementioned process via its coordination affinity with the zinc ions in the complex species of Zn(II)-citrate.

According to the above analysis and description, the formation mechanism of the as-prepared monodispersed flaky dihydrate zinc oxalate particles can be summarized using the following chemical expressions:

$$Zn^{2+}\text{–Citrate} \rightarrow Zn^{2+} + \text{Citrate} \quad (1)$$

$$Zn^{2+} + C_2O_4^{2-} + 2H_2O \rightarrow ZnC_2O_4{\cdot}2H_2O_{(s)} \quad (2)$$

During the precipitation process, zinc ions will be slowly released from the complex of Zn(II)–citrate and precipitate in the form of hydrate zinc oxalate particles. In this process, the citrate ligand may be absorbed into the surface of the nuclei or crystal subunits, causing the aggregation to orient into larger particles with a flaky morphology due to its selective anchoring on the special crystal facet of the hydrate zinc oxalates. It can be deduced that the citrate plays multiple roles in the precipitation system, including being a chelating agent, shape tuning agent, and dispersing agent. During the precipitation process, it was observed that the induction time for the first nucleation during the experimental process was approximately 10 h, indicating that the solution system is a very typical slow-reaction synthesis process, which is very favorable for skipping the secondary nucleation in the growth stage and finally producing the monodispersed particles.

4. Conclusion

The micron-sized dihydrate zinc oxalate particles with a flaky morphology could be prepared by performing a simple precipitation reaction of sodium oxalate with zinc nitrate in the absence and presence of citrate ligand both as a crystalline tailoring reagent and nucleation inhibitor. The concentration of citrate and the pH value of the solution are proven to be the most significant parameters to achieve morphological control of zinc oxalate particles. A high citrate concentration generally resulted in large particles by selective adsorption on the special crystal facet of the zinc oxalate particles, which further caused the formation of a flaky morphology. A medium pH value of approximately 6–7 was

suitable to perform morphological tailoring. Such a shape evolution may provide a novel insight about the morphological control of dihyrate zinc oxalate particles and the controllable synthesis of other novel inorganic materials.

Acknowledgement

The authors want to thank Dr. Li from the China Academic Institute of Automatics for his help during SEM observations.

References

[1] R. Kumar, A. Umar, G. Kumar, and H.S. Nalwa, Antimicrobial properties of ZnO nanomaterials: A review, *Ceram. Int.*, 43(2017), No. 5, p. 3940.

[2] Q. Nie, L. Yang, C. Cao, Y.M. Zeng, G.Z. Wang, C.Z. Wang, and S.W. Lin, Interface optimization of ZnO nanorod/CdS quantum dots heterostructure by a facile two-step low-temperature thermal treatment for improved photoelectrochemical water splitting, *Chem. Eng. J.*, 325(2017), p. 151.

[3] L.P. Wang, F. Zhang, S. Chen, and Z.H. Bai, One-pot synthesis and optical properties of In- and Sn-doped ZnO nanoparticles, *Int. J. Miner. Metall. Mater.*, 24(2017), No. 4, p. 455.

[4] J.H. Zhou, C.D. Pu, T.Y. Jiao, X.Q. Hou, and X.G. Peng, A two-step synthetic strategy toward monodisperse colloidal CdSe and CdSe/CdS core/shell nanocrystals, *J. Am. Chem. Soc.*, 138(2016), No. 20, p. 6475.

[5] A. Umar, J. Lee, J. Dey, and S.M. Choi, Seedless synthesis of monodisperse cuboctahedral gold nanoparticles with tunable sizes, *Chem. Mater.*, 28(2016), p. 4962.

[6] X.L. Hu, J.M. Gong, L.Z. Zhang, and J.C. Yu, Continuous size tuning of monodisperse ZnO colloidal nanocrystal clusters by a microwave-polyol process and their application for humidity sensing, *Adv. Mater.*, 20(2008), No. 24, p. 4845.

[7] K. Kanie, Y. Seino, M. Matsubara, and A. Muramatsu, Size-controlled hydrothermal synthesis of monodispersed $BaZrO_3$ sphere particles by seeding, *Adv. Powder Technol.*, 28(2017), p. 55.

[8] D.S. Wang, X.L. Ma, Y.G. Wang, L. Wang, Z.Y. Wang, W. Zheng, X.M. He, J. Li, Q. Peng, and Y.D. Li, Shape control of CoO and $LiCoO_2$ nanocrystals, *Nano Res.*, 3(2010), No. 1, p. 1.

[9] L.V. Trandafilović, R.K. Whiffen, S. Dimitrijević-Branković, M. Stoiljković, A.S. Luyt, and V. Djoković, ZnO/Ag hybrid nanocubes in alginate biopolymer: Synthesis and properties, *Chem. Eng. J.*, 253(2014), p. 341.

[10] S. Watanabe, S. Ohsaki, T. Hanafusa, K. Takada, H. Tanaka, K. Mae, and M.T. Miyahara, Synthesis of zeolitic imidazolate framework-8 particles of controlled sizes, shapes, and gate adsorption characteristics using a central collision-type microreactor, *Chem. Eng. J.*, 313(2017), p. 724.

[11] V.K. LaMer and R.H. Dinegar, Theory, production and mechanism of formation of monodispersed hydrosols, *J. Am. Chem. Soc.*, 72(1950), No. 11, p. 4847.

[12] P.P. von Weimarn, The precipitation laws, *Chem. Rev.*, 2(1926), No. 2, p. 217.

[13] J. Tóth, A. Kardos-Fodor, and S. Halász-Péterfi, The formation of fine particles by salting-out precipitation, *Chem. Eng. Process*., 44(2005), No. 2, p. 193.

[14] A. Seyed-Razavi, I.K. Snook, and A.S. Barnard, Origin of nanomorphology: does a complete theory of nanoparticle evolution exist?, *J. Mater. Chem.*, 20(2010), No. 3, p. 416.

[15] D.T. Nguyen and K.S. Kim, Self-development of hollow TiO_2 nanoparticles by chemical conversion coupled with Ost wald ripening, *Chem. Eng. J.*, 286(2016), p. 266.

[16] S.G. Kwon and T. Hyeon, Formation mechanisms of uniform nanocrystals via hot-injection and heat-up methods, *Small*, 7(2011), No. 19, p. 2685.

[17] J. Park, J. Joo, S.G. Kwon, Y.J Jang, and T. Hyeon, Synthesis of monodisperse spherical nanocrystals, *Angew. Chem. Int. Ed.*, 46(2007), p. 4630.

[18] V. Sebastian, C.D. Smith, and K.F. Jensen, Shape-controlled continuous synthesis of metal nanostructures, *Nanoscale*, 8(2016), No. 14, p. 7534.

[19] L.M. Yang, K.E. Knowles, A. Gopalan, K.E. Hughes, M.C. James, and D.R. Gamelin, One-pot synthesis of monodisperse colloidal copper-doped CdSe nanocrystals mediated by ligand–copper interactions, *Chem. Mater.*, 28(2016), No. 20, p. 7375.

[20] T. Wang, L.Y. Zhang, H.Y. Wang, W.C. Yang, Y.C. Fu, W.L. Zhou, W.T. Yu, K.S. Xiang, Z. Su, S. Dai, and L.Y. Chai, Controllable synthesis of hierarchical porous Fe_3O_4 particles mediated by poly(diallyldimethylammonium chloride) and their application in arsenic removal, *ACS Appl. Mater. Interfaces*, 5(2013), No. 23, p. 12449.

[21] S.J. Kim, Y.T. Kim, and J. Choi, Facile and rapid synthesis of zinc oxalate nanowires and their decomposition into zinc oxide nanowires, *J. Cryst. Growth*, 312(2010), No. 20, p. 2946.

[22] J. Kaur, S. Bansal, and S. Singhal, Photocatalytic degradation of methyl orange using ZnO nanopowders synthesized via thermal decomposition of oxalate precursor method, *Physica B*, 416(2013), p. 33.

[23] Z.J. Gao, Y.S. Gu, X.Q. Wang, and Y. Zhang, Mechanical properties of Mn-doped ZnO nanowires studied by first-principles calculations, *Int. J. Miner. Metall. Mater.*, 19(2012), No 1, p. 89.

[24] M. Shamsipur, M. Roushani, and S.M. Pourmortazavi, Electrochemical synthesis and characterization of zinc oxalate nanoparticles, *Mater. Res. Bull.*, 48(2013), No. 3, p. 1275.

[25] Z.G. Jia, L.H. Yue, Y.F. Zheng, and Z.D. Xu, Rod-like zinc oxide constructed by nanoparticles: synthesis, characterization and optical properties, *Mater. Chem. Phys*., 107(2008), No. 1, p. 137.

[26] L. Ni, L. Wang, B. Shao, Y.J. Wang, WL. Zhang, and Y. Jiang, Synthesis of flower-like zinc oxalate microspheres in ether-water bilayer refluxing systems and their conversion to zinc oxide microspheres, *J. Mater. Sci. Technol.*, 27(2011), No. 6, p. 563.

[27] T. Tang and T.Z. Yang, *Fundamental and Technology of Complex Metallurgy*, Central South University Press, Changsha, 2011, p. 4.